annalen der physik
www.ann-phys.org

Modeling the Ultrafast Response of Two-Magnon Raman Excitations in Antiferromagnets on the Femtosecond Timescale

*Giovanni Batignani, Emanuele Pontecorvo, Davide Bossini, Carino Ferrante, Giuseppe Fumero, Giulio Cerullo, Shaul Mukamel, and Tullio Scopigno**

Illuminating a magnetic material with femtosecond laser pulses induces complex ultrafast dynamical processes. The resulting optically detectable response usually contains contributions from both the optical properties and the magnetic degrees of freedom. Disentangling all the different components concurring to the generation of the total signal is a major challenge of contemporary experimental solid-state physics. Here, this problem is tackled, addressing the purely optical, nonmagnetic artifacts on the time resolved two-magnon stimulated Raman spectrum of an antiferromagnet, rationalizing the recent observation on the exchange energy modification upon photo-excitation. It is demonstrated how the genuine dynamics of the magnetic eigenmode can be disentangled from the nonlinear optical effects, generated by cross phase modulation, on the femtosecond timescale. The introduced approach can be extended for the investigation of <100 fs dynamic processes by means of coherent Raman scattering.

The demand for devices able to store and encode information at ever-increasing speed, in parallel with the advent of bright femtosecond laser sources have been instrumental for the development of ultrafast magnetism.[1,2] Since the early experiments investigating ultrafast spin dynamics, it has been clear that ultrashort laser pulses trigger many complicated pathways of energy and angular momentum transfer between photons, electrons, the lattice, and spins.[3–5] The observed phenomena, such as ultrafast demagnetization,[3] all-optical switching,[4,6] photoinduced magnetic phase transitions,[7,8] and the impulsive generation of coherent magnons[5,9,10] have been hitherto discussed mainly in terms of spin–orbit coupling perturbations.[1,2] Critically, the role of the exchange interaction, which is the strongest magnetic interaction responsible for magnetic order, has been only barely taken into account,[11,12] due to the lack of direct ultrafast optical probes of the exchange energy. Hence, developing an experimental method and protocol able to unambiguously reveal the photoinduced dynamics of the exchange energy, void from any optical effects, would reveal an unexplored regime of magnetic phenomena.

Raman scattering represents a powerful tool for investigating magnetic excitations (magnons) in ferromagnetic and antiferromagnetic systems at equilibrium[13,14] as well as for accessing transient magnetic phases in time-resolved experiments.[15,16] However, due to the time-energy resolution restrictions dictated by the Fourier transform limit,[17,18] spontaneous Raman (SR) spectroscopies are ineffective on sub-picosecond time regimes and in particular cannot access the dynamical response of the exchange interaction. Time-resolved femtosecond stimulated

Dr. G. Batignani, Dr. E. Pontecorvo, Dr. C. Ferrante, Dr. G. Fumero, Prof. T. Scopigno
Dipartimento di Fisica
Universitá di Roma "La Sapienza"
I-00185 Roma, Italy
E-mail: tullio.scopigno@uniroma1.it
Dr. D. Bossini
Institute for Molecules and Materials
Radboud University Nijmegen
6525 AJ Nijmegen, The Netherlands
Dr. D. Bossini
Experimentelle Physik VI
Technische Universität Dortmund
44221 Dortmund, Germany

The ORCID identification number(s) for the author(s) of this article can be found under https://doi.org/10.1002/andp.201900439

DOI: 10.1002/andp.201900439

Dr. C. Ferrante, Prof. T. Scopigno
Istituto Italiano di Tecnologia
Center for Life Nano Science @Sapienza
I-00161 Roma Italy
Dr. G. Fumero
Dipartimento di Scienze di Base e Applicate per l'Ingegneria
Universitá di Roma "La Sapienza"
I-00161 Roma Italy
Prof. G. Cerullo
IFN-CNR, Dipartimento d Fisica
Politecnico di Milano
P.zza L. da Vinci 32, 20133 Milano, Italy
Prof. S. Mukamel
Department of Chemistry
University of California
Irvine, CA 92697, USA

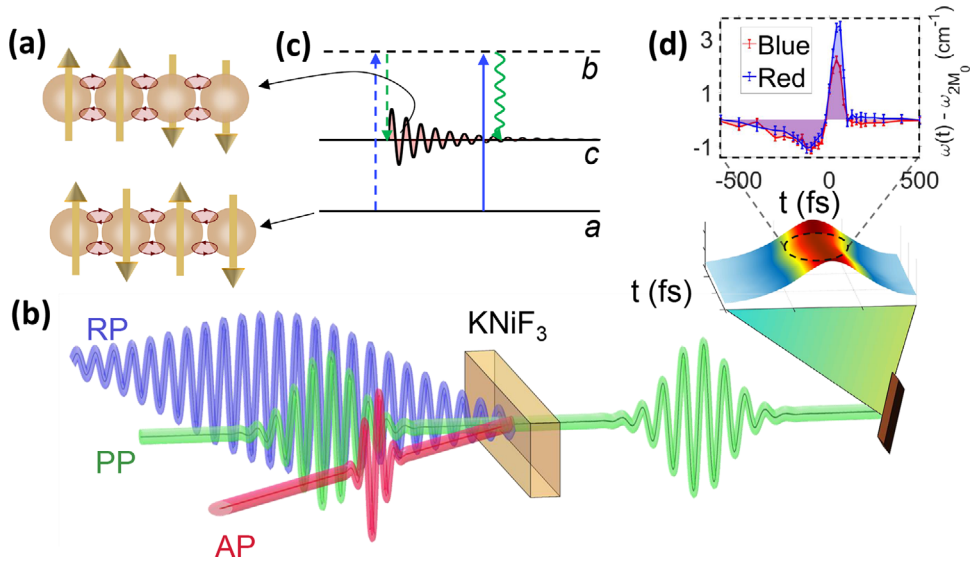

Figure 1. Sketch of the time-resolved FSRS experimental scheme for probing magnon dynamics in $KNiF_3$. a,b) Two-magnon excitations are coherently stimulated by the joint action of a picosecond RP and a broadband femtosecond PP, that generates two spin flip events occurring on neighboring sites. A further interaction with the RP followed by a final free induction decay enables to probe the excited magnons as Raman gain or Raman loss. In panel c), we report the energy ladder diagram representing the SRS interaction in the red side, where *a* indicates the ground state, *b* represents a virtual electronic level, while *c* is a two magnon excited state. The presence of an AP pulse triggers the dynamics of interest and, at the same time, modifies the Raman spectrum due to cross-phase modulation with the RP. d) By varying the time delay between AP and RP–PP pair, the photoinduced modification of the 2ML peak position can be monitored. All the pulses are tuned off-resonant with the sample absorption, ensuring that electrons are not excited upon photo-irradiation.

Raman scattering (FSRS)[19,20] is a powerful technique that can overcome such limitations.[21–26] By combining a narrowband Raman pulse (RP) with a femtosecond broadband probe pulse (PP), illuminating the sample following an actinic pump (AP) photoexcitation, time-resolved FSRS is able to coherently stimulate and subsequently record out-of-equilibrium Raman excitations both in molecular and solid-state systems.[27–35] For example, FSRS has been recently exploited for investigating the lattice dynamics in semiconductor nanocrystals[36] and the ultrafast long-range charge separation in polymeric semiconductors,[37] while impulsive stimulated Raman scattering, performed in time-domain instead of frequency domain, has been used for studying photo-carrier dynamics in hybrid perovskites.[38–40] The combination of the narrowband RP with the femtosecond PP, acting as probe pulses, ensures uncompromised spectral resolution (a few wavenumbers) and temporal precision (down to 50 fs).[41–43] Recently, time-resolved FSRS has been used for studying the photoinduced magnon excitation dynamics, extracting the modification of the exchange interaction in the insulating cubic perovskite $KNiF_3$ on the femtosecond timescale.[44,45] Critically, since the dynamics under investigation was entirely generated during the temporal overlap of the pump and probe pulses, the transient Raman spectra were dominated by the presence of purely optical, off-resonant nonlinear processes, usually referred to as coherent artifact,[46–50] which obscure the genuine exchange energy dynamics.

The optical artifact was indirectly removed from the time-resolved Raman spectra, building on a comparison between the contributions to the spectrum shifted to the red and blue wavenumbers (conventionally referred as Stokes and anti-Stokes sides in spontaneous Raman spectroscopy) with respect to the RP central frequency.[51,52] Indeed, since the experiment was performed in nonresonant condition, the effect of the artifact on the fifth order nonlinear response was the same in the red and in the blue side of the time-resolved FSRS spectrum,[44,45] while the signatures of the exchange dynamics contributed differently to the two sides. This is not always true and this procedure cannot be extended to resonant time-resolved FSRS experiments or to cases where the red and blue sides of the spectrum cannot be simultaneously measured under the same conditions. In this work, we assign the origin of the nonresonant fifth-order process to cross phase modulation (XPM)[50,53,54] between the RP and the AP pulses. Selecting the paradigmatic case of the antiferromagnetic dielectric $KNiF_3$, we show how to model it based on the spectral profile of two-magnon line excitations, factoring out from the total time-resolved FSRS signal and recovering the genuine dynamics of the exchange interaction. Our model allows to derive a protocol for the analysis of FSRS spectra that can be extended to many solid-state systems, disclosing the power of the FSRS technique to the condensed matter community.

The FSRS experimental scheme, used for accessing the magnetic properties of $KNiF_3$ and its ultrafast response, is sketched in **Figure 1**b. Details of the experimental setup are reported in ref [44].

Briefly, a 650 nm, horizontally polarized, 60 fs AP pulse with 60 mJ cm^{-2} fluence photo-excites the system, which is then probed by the joint action of a vertically polarized RP (500 nm, 5 mJ cm^{-2}, 5 cm^{-1} bandwidth, ≈3 ps time duration) and a broadband PP. All the pulses are off-resonantly tuned with respect to the sample absorption, in order to ensure that hot electrons are not generated upon photo-irradiation. By tuning the relative delay between the AP and the RP–PP pair, it is possible to monitor

the dynamics of the Raman excitations. The sample, a 340 μm-thick (100) plane-parallel plate, is antiferromagnetically ordered below the Néel point $T_N = 246$ K and it is maintained at the temperature $T = 77$ K during the time-resolved FSRS experiment by means of a cryostat. The antiferromagnetic order in $KNiF_3$ arises from the super-exchange interaction between nearest neighbors Ni^{2+} ions,[55] mediated by the nonmagnetic F^- ions. Raman spectroscopy can directly access the exchange energy in this sample, being able to simultaneously excite two magnons on different sublattices in the high-wavevector region of the magnon dispersion.[14,56] According to the Heisenberg-exchange Hamiltonian

$$\hat{H}_{ex} = \frac{1}{2}\sum_{a\neq b} J_{ab}\,\langle \hat{\mathbf{S}}_a \cdot \hat{\mathbf{S}}_b \rangle \tag{1}$$

describing such elementary magnetic excitation, the energy of the 2 magnon line (2ML) excitation[57,58] (Figure 1a), generated by two spin flip events (with the total spin S of the system unchanged) occurring on neighboring sites, can be expressed as $\hbar\omega_{2ML} = \frac{2nS-1}{S^2} J_{ab}\,\langle \hat{S}_a \hat{S}_b \rangle$, which is directly proportional to the exchange interaction. Here, n is the number of nearest neighbors. Measuring the 2ML position can thus be used to directly access the exchange energy.

The AP induced modification of the 2ML peak position as a function of the relative delay between AP and PP is reported in Figure 1d, for both the red and the blue sides of the FSRS spectrum measured under the same experimental conditions (i.e., with the same pulse fluences, energies, and wavelengths). Notably, for positive time delays, the peak shift detected within the temporal overlap between AP and PP is not the same for the blue and red sides of the RP and is at odds with what is expected for a purely dynamical effect, that is, a light-induced modification of the 2M frequency. In fact, the Raman peak shifts to the right on both sides of the spectrum (i.e., to red-shifted wavelengths), but this indicates a light-induced decrease of the 2M frequency in the red side and an increase in the blue side, since the two sides are defined with respect to the RP frequency. Moreover, a peak shift, with the same amplitude and opposite sign in terms of Raman shift, occurs also at negative time delays, when the 2M frequency is still unaffected by the actinic photo-excitation. The overall response can be interpreted as the sum of two concurring processes: a dynamical modification of the exchange interaction and a purely optical nonresonant process, altering the time-resolved FSRS spectral lineshape and obscuring the genuine 2ML modification.

As depicted in the diagram of Figure 1c, the spatial and temporal overlap of the RP–PP pair generates the two spin flip events and stimulates the two-magnon excitations (Figure 1a). The coherent stimulation requires the temporal overlap of the picosecond RP and the femtosecond PP. Therefore the temporal precision in the generation of the Raman coherences is dictated by the duration of the probe, while the spectral resolution is determined by the RP spectrum.[41,42] A further interaction with the RP and a free induction decay enables to probe the excited magnons as 2ML loss and gain peaks over the PP spectrum.

Adding an AP photo-excitation to this two pulse stimulated Raman scattering experimental layout, for triggering the dynamics of the exchange interaction, enables to acquire time-resolved FSRS spectra. Critically, the presence of the AP will result also in the generation of XPM induced artefacts, which are due to the AP-induced modifications of the RP and are superimposed to the FSRS genuine dynamics.[20] In this respect, we note that, considering the SRS process exploited for probing the system out-of-equilibrium dynamics, while the first interaction with the RP (first vertical dashed arrow in Figure 1c) takes place during the temporal overlap between Raman and probe pulses (i.e., on a 50 fs timescale), the latter interaction with the RP (vertical continuous arrow in Figure 1c) occurs within the dephasing time of the stimulated 2ML coherence and the residual duration of the RP.[59,60] As a result, XPM between the AP and the RP can affect the spectral response not only during the temporal overlap of the AP–PP pair, but also for negative time delays, that is, for an AP following the PP, inducing different distortion in the FSRS lineshape.

In the absence of the AP, the stimulated Raman scattering (SRS) can be expressed in terms of the third order polarization.[17,61–63] Considering the simple three-level model system shown in Figure 1 and an exponentially damped harmonic mode, with frequency ω_{ca} and inverse lifetime Γ_{ca}^{-1}, the frequency dispersed third order polarization accounting for the SRS signal on the red side of the Raman pulse can be expressed as

$$P^{(3)}(\omega) = |\mu_{ab}|^2|\mu_{bc}|^2 \frac{1}{\omega - \tilde{\omega}_{bc}} \int_{-\infty}^{\infty} d\omega_1 \frac{\mathcal{E}_R^*(\omega_1)}{\omega_R + \omega_1 + \tilde{\omega}_{ab}} \times \int_{-\infty}^{\infty} d\omega_3 \frac{\mathcal{E}_R(\omega_3)\mathcal{E}_P(\omega - \omega_P + \omega_1 - \omega_3)}{\omega - \omega_3 - \omega_R - \tilde{\omega}_{ac}} \tag{2}$$

where $\tilde{\omega}_{ij} = \omega_i - \omega_j - i\Gamma_{ij}$ and μ_{ij} represents the dipole transition moment between the i and j states.

The PP modifications, induced in presence of a nonlinear polarization in the material, can be hence calculated by numerically integrating the wave equation (Equation (S5), Supporting Information), obtaining the resulting stimulated Raman gain (SRG) spectrum as

$$\mathrm{SRG} = \frac{|E_P(\omega, L) - E_P(\omega, 0)|^2}{|E_P(\omega, 0)|^2} \tag{3}$$

The XPM effect between two laser fields $E_i(z,t)$ and $E_j(z,t)$ can be described by the coupled nonlinear Schrödinger equations[54]

$$\begin{aligned} \frac{\partial A_i}{\partial z} + \frac{i}{2}\beta_2^{(i)}\frac{\partial^2 A_i}{\partial \tau^2} &= i\gamma\left(|A_i|^2 + 2|A_j|^2\right)A_i \\ \frac{\partial A_j}{\partial z} + \epsilon\frac{\partial A_j}{\partial \tau} + \frac{i}{2}\beta_2^{(j)}\frac{\partial^2 A_j}{\partial \tau^2} &= i\gamma\left(|A_j|^2 + 2|A_i|^2\right)A_j \end{aligned} \tag{4}$$

where we have considered the linear ($\beta_1^{(i)} = \frac{dk}{d\omega}|_{\omega=\omega_i} = v_g^{-1}$) and the quadratic ($\beta_2^{(i)} = \frac{d^2k}{d\omega^2}|_{\omega=\omega_i}$) dispersion effects, the group-velocity mismatch parameter $\epsilon = \beta_1^{(i)} - \beta_1^{(j)}$, and adopted a moving temporal frame $\tau = t - \beta_1^{(i)} z$. In Equation (4), γ takes into account for the coupling, through cross-phase modulation, between optical fields propagating in a nonlinear medium.[54,64,65] The optical electric field $E_j(z,t)$, propagating along the z direction, has been represented as $E_j(z,t) = A_j(z,t)e^{i(k_j z - \omega_j t)}$. As shown in **Figure 2**, in the presence of XPM, the RP phase is modulated as a function of

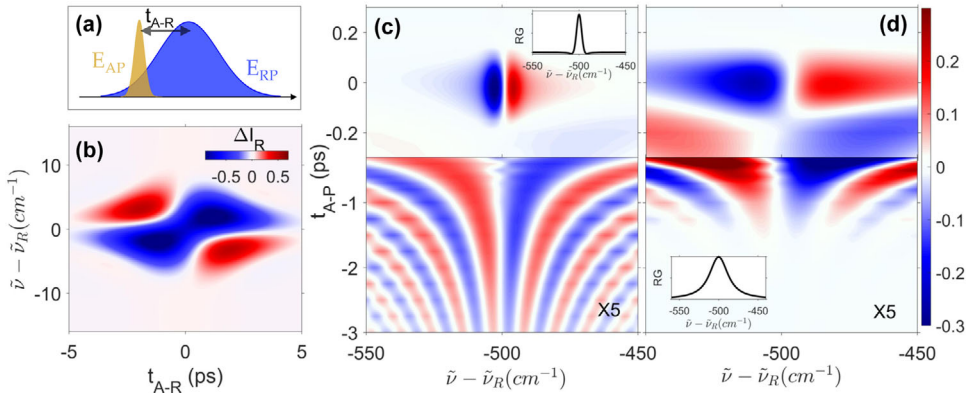

Figure 2. Cross phase modulation artifacts: the Raman pulse phase is modulated as a function of the time delay t_{A-R} between AP and RP (a) due to XPM between the two pulses. The resulting spectral modification of the RP is shown in (b), where we report the differential RP spectrum ΔI_R, that is, the RP spectral profile measured with and without the presence of the AP. In (c), the corresponding differential steady-state FSRS spectrum $\Delta FSRS(\omega, t_{A-P})$ is calculated for a Raman line at 500 cm^{-1}, with $\Gamma_{ca}^{-1} = 8$ ps, as a function of the relative delay t_{A-P} between the AP and PP (with temporal delay between the PP and RP fixed). The unperturbed SRS spectral lineshape is reported in the sub-panel by the black line. $\Delta FSRS(\omega, T_{A-P})$ measured at negative time delays ($t_{A-P} < -300$ fs), that is, for an AP following the PP, has been scaled by a factor 5. In (d), we report the same differential steady-state FSRS spectrum $\Delta FSRS(\omega, t_{A-P})$ for a Raman line at 500 cm^{-1}, considering the case of a much faster dephasing time, that is, $\Gamma_{ca}^{-1} = 400$ fs. For negative time delays, an oscillating profile covers a large spectral region, broader than the Raman line-width, and lasts for a time interval within the vibrational dephasing time and the residual duration of the RP. During the temporal overlap between AP and PP, we observe an asymmetric dispersive feature centered around the Raman peak, resulting in a red-shift of the peak position.

the RP–AP temporal delay t_{A-R}, resulting in a transformation of the spectral properties of the RP (Figure 2b).[66]

The specific way XPM shows up in spectral artifacts affecting the time-resolved FSRS signal can be numerically calculated by integrating the wave equation, with the field envelopes evaluated at each point across the sample accordingly to Equation (4). In Figure 2c, we report the computed off-resonance differential signal $\Delta FSRS(\omega, t_{A-P})$, in the red side, defined as the difference of the FSRS spectra measured in the presence and absence of the AP, for an ideal harmonic mode, with $\omega_{ca} = 500$ cm^{-1} and $\Gamma_{ca}^{-1} = 8$ ps. The simulation has been performed for a 3 ps RP, with the PP preceding the RP (1 ps temporal delay). The pulses temporal ordering chosen in the simulation, with the RP following the PP, represents the typical experimental layout for the SRS and FSRS schemes, providing the optimal trade-off in terms of spectral resolution and maximum of Raman Gain.[59,60] Within the AP–PP temporal overlap, XPM causes a dispersive profile, which alters the measured peak position, inducing an apparent red-shift. On the contrary, for negative time delays t_{A-P}, an oscillating profile can induce a blue-shift of the measured peak position. Notably, if $t_{A-P} < 0$, the time-resolved FSRS response does not bear any information on the photoinduced transient dynamics, with the spectral modifications entirely ascribed to XPM induced artifacts; therefore, the FSRS response at negative delays can be exploited to calibrate the parameters required to model the XPM induced artifact, which can be subsequently removed from the FSRS spectrum over the entire pump probe delay window (i.e., for any value of t_{A-P}). We note that the spectral modulation at negative time delays shows an amplitude less intense than the dispersive profile at positive time delays and a frequency which is inversely proportional to t_{A-P}. Moreover, it lasts for a time interval comprised within the vibrational dephasing time and the residual duration of the RP. For these reasons, a correct estimation of the induced peak shift has to precisely take into account the spectral profile of the SRS signal and the dephasing time of the Raman modes under investigation. A convenient way to model the physical parameters of magnon excitations ruling their peculiar Raman lineshapes is to consider a microscopic description of the magnon Raman scattering events in terms of the second-order Green function formalism presented in ref. [67], which enables to obtain magnon self-energies, consistently taking into account finite magnon lifetimes and reproducing their Raman spectral profile. For boundary region magnons (i.e., magnons whose wavevectors lie near the edges of the first Brillouin zone), the spontaneous Raman cross section can be expressed as[14]

$$K(\omega) = \frac{C}{1 - e^{-\hbar\omega/(k_B T)}} \alpha^2(T) S^2 \left(-\frac{1}{2\pi}\right) \Im[G_{2ML}(\omega)] \tag{5}$$

where $\alpha(T)$ is the renormalization Hartree–Fock factor and the constant C contains all the polarization dependence, together with the interacting light electric fields. The propagator $G_{2ML}(\omega)$ is

$$G_{2ML}(\omega) = \frac{L_0(\omega)}{1 - JL_0(\omega)} \tag{6}$$

For the simple cubic $KNiF_3$ lattice,[13] we have

$$\begin{aligned} L_0(\omega) = & -\frac{3}{\pi JSn} \int_0^1 dx \frac{x}{\sqrt{1-x^2}} \\ & \times \frac{\coth\left[\frac{1}{2}(JSn/k_B T_N)\alpha(T/T_N)(xT_N/T)\right]}{\omega/(2JSn) - \alpha(T/T_N) + i\Gamma'/(JSn)} \\ & \times \left\{ C_{000}\left[3\left(1-x^2\right)^{1/2}\right] - C_{200}\left[3\left(1-x^2\right)^{1/2}\right] \right. \\ & \left. + 2C_{110}\left[3\left(1-x^2\right)^{1/2}\right] \right\} \end{aligned} \tag{7}$$

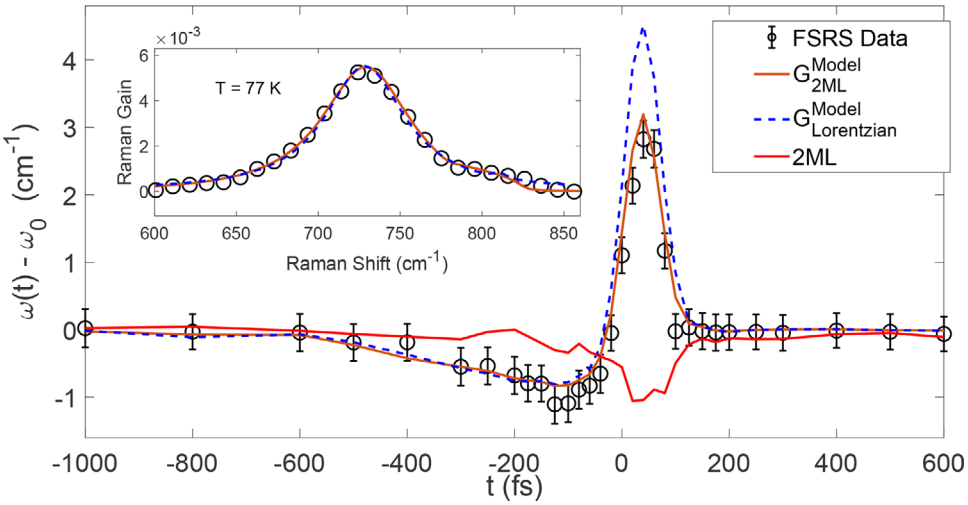

Figure 3. Photoinduced evolution of the Raman shift of the 2M line in the time-resolved FSRS spectra arising from XPM induced artifacts as a function of actinic pump delay. The black line reports the experimental XPM signal, which has been evaluated as the sum of the red and blue side peak shifts, in order to cancel out effects arising from a modification of the exchange energy. Inset: stimulated Raman scattering on $KNiF_3$. FSRS and SRS spectra are simulated both using the sum of Lorentzian contributions (blue dashed lines) and building on the microscopic description of the magnon Raman scattering events in terms of the second-order Green function formalism (continuous orange line). Although modeling the Raman response as a sum of Lorentzian contributions can reproduce the steady-state SRS spectrum, it fails for extracting the XPM induced artifacts, which, on the contrary, are reproduced by the orange line. The genuine dynamics of the 2M line, modified due to the light induced manipulation of the exchange interaction, can be retrieved by subtracting the XPM induced artifact and is reported by the red line.

Here, $n = 6$ is the number of nearest neighbors, $S = 1$, $J = 70.5\,\mathrm{cm}^{-1}$, T_N is the Neel temperature, $T = 77$ K, $\Gamma'/(JSn) = 3 \cdot 10^{-3}$, $\alpha(T = 77\,\mathrm{K}) \approx 0.977$, and $C_{ijk}(z)$ are defined by means of Bessel functions $J(i)$

$$C_{ijk}(z) = \int_0^\infty dt \cos(zt) J_i(t) J_j(t) J_k(t)$$

The $KNiF_3$ stimulated Raman response can be expressed substituting the propagator $\frac{1}{(\omega-\omega_3-\omega_R-\tilde{\omega}_{ac})}$ with $G_{2ML}(\omega-\omega_3-\omega_R)$ in Equation (2)[17]

$$P^{(3)}(\omega) = \frac{|\mu_{ab}|^2|\mu_{bc}|^2}{\omega-\tilde{\omega}_{bc}} \int_{-\infty}^{\infty}\int_{-\infty}^{\infty} d\omega_1 d\omega_3 \times \frac{\mathcal{E}_R^*(\omega_1)\mathcal{E}_R(\omega_3)\mathcal{E}_P(\omega-\omega_P+\omega_1-\omega_3)G_{2ML}(\omega-\omega_3-\omega_R)}{\omega_R+\omega_1+\tilde{\omega}_{ab}} \quad (8)$$

The simulated SRS spectrum is shown in the inset of **Figure 3** (orange continuous line) and is in agreement with the experimental result (black circles).

In order to assess the reliability of the proposed framework for reproducing the XPM induced artifact, we compared the XPM-induced frequency shift of the FSRS peak position $\Delta\omega(t) = \omega(t) - \omega_0$ (evaluated by Equations (4) and (8)) with an indirect determination obtained by isolating the XPM as the average of the red and blue Raman shifted components (the 2ML dynamics is in this way factored out[44]). In this respect, as we have previously mentioned, the parameters required for modeling the FSRS artifact have been calibrated using only the negative time delays region ($t < -100$ fs). The results shown in Figure 3 reveal that the experimental (black circles) $\Delta\omega(t)$ profile is well reproduced by the simulated one (orange line). By subtracting the calculated XPM signal from the time-resolved FSRS trace measured in the red side of the spectrum, we can finally retrieve the genuine 2ML peak shift due to the light induced manipulation of the exchange interaction, which is $\approx 1\,\mathrm{cm}^{-1}$.

It is now worth assessing the impact of an accurate modeling of the static excitation spectral profiles on the reproduced XPM contribution. To this aim, we compared the signal obtained using the microscopic description of the two-magnon Raman scattering in terms of the second-order Green function formalism discussed so far with the one extracted using a sum of standard Lorentzian profiles, with lifetimes obtained fitting the steady-state Raman spectrum (blue dashed line in the inset of Figure 3). Importantly, the XPM profile obtained with this latter strategy is significantly different and is not able to reproduce the experimental peak shift. This demonstrates how the peculiarities of the elemental excitations of interest—the two-magnon line in the present case—are critically relevant to retrieve accurate information on the FSRS ultrafast dynamics.

Importantly, the presented approach for recovering the genuine system dynamics in time-resolved FSRS spectra offers a procedure for factoring out nonlinear artifacts without the need of resorting to ad hoc workaround,[44] only applicable in the off-resonant condition.

In this paper, we have introduced a novel protocol for the analysis of FSRS spectra which allows to disentangle genuine ultrafast dynamics from XPM artifacts. The protocol is based on the following strategy:

- Obtaining the physical parameters (self-energies and lifetime) of the specific excitation of interest from static Raman measurements using the appropriate lineshape modeling. We have indeed shown how the effect of the XPM artifact on the

FSRS-determined dynamics of a quasi-particle critically depends upon its nature.
- Exploiting the negative delays FSRS spectra, which do not bear any information on the material dynamics, to calibrate all the parameters required to calculate the XPM artifact, by combining Equations (4) and (8).

This scheme, illustrated in the paradigmatic case of two-magnon excitations in the insulating cubic perovskite $KNiF_3$, allows to factor out the isolated XPM induced artifact and to retrieve accurate information on the ultrafast dynamics buried beneath the raw FSRS signals. The present approach can be exploited for disclosing the real dynamics of complex Raman lines on timescales as short as the duration of the femtosecond AP and PP pulses by means of time-resolved FSRS.

We anticipate that this strategy will pave the way to the application of FSRS to the study of the photoinduced ultrafast dynamics of high-energy one-magnon or two-magnon excitations in a broad range of solid-state magnetic materials,[56] such as transition metal oxides (NiO, CoO, or MnO), binary fluorides (FeF_2 or NiF_2), trifluorides (e.g., $NaNiF_3$ and KNi_2F_4 as well as the already studied $KNiF_3$), strongly correlated iridates (e.g., Sr_2IrO_4), and even high-temperature cuprate superconductors (such as YBCO or BSCCOs), where the high-energy spin excitations, related to the two-magnon mode, were shown to play a major role in the mechanism that allows the high-temperature superconductivity.[68]

Acknowledgements

This research was partially supported by de Nederlandse Organisatie voor Wetenschappelijk Onder-zoek (NWO), de Stichting voor Fundamenteel Onderzoek der Materie (FOM), and the European Research Council under the European Union's Seventh Framework Program (FP7/2007-2013)/ERC Grant Agreement No. 257280 (Femtomagnetism). S.M. gratefully acknowledges the support of the National Science Foundation (Grant No. CHE-1663822). G.B. acknowledges the "Avvio alla ricerca 2018" grant by Sapienza Universitá di Roma.

Conflict of Interest

The authors declare no conflict of interest.

Keywords

coherent Raman, light–matter interaction, nonlinear optics, ultrafast photonics

Received: September 24, 2019
Revised: October 14, 2019
Published online: November 18, 2019

[1] A. Kirilyuk, A. V. Kimel, T. Rasing, *Rev. Mod. Phys.* **2010**, *82*, 2731.
[2] D. Bossini, T. Rasing, *Phys. Scr.* **2017**, *92*, 024002.
[3] E. Beaurepaire, J. C. Merle, A. Daunois, J. Y. Bigot, *Phys. Rev. Lett.* **1996**, *76*, 4250.
[4] C. D. Stanciu, F. Hansteen, A. V. Kimel, A. Kirilyuk, A. Tsukamoto, A. Itoh, T. Rasing, *Phys. Rev. Lett.* **2007**, *99*, 047601.
[5] A. V. Kimel, A. Kirilyuk, P. A. Usachev, R. V. Pisarev, A. M. Balbashov, T. Rasing, *Nature* **2005**, *435*, 655.
[6] A. Stupakiewicz, K. Szerenos, D. Afanasiev, A. Kirilyuk, A. V. Kimel, *Nature* **2017**, *542*, 71.
[7] D. Afanasiev, B. Ivanov, A. Kirilyuk, T. Rasing, R. Pisarev, A. Kimel, *Phys. Rev. Lett.* **2016**, *116*, 097401.
[8] D. Bossini, K. Konishi, S. Toyoda, T. Arima, J. Yumoto, M. Kuwata-Gonokami, *Nat. Phys.* **2018**, *14*, 370.
[9] N. Kanda, T. Higuchi, H. Shimizu, K. Konishi, K. Yoshioka, M. Kuwata-Gonokami, *Nat. Commun.* **2011**, *2*, 362.
[10] T. Kampfrath, A. Sell, G. Klatt, A. Pashkin, S. Mährlein, T. Dekorsy, M. Wolf, M. Fiebig, A. Leitenstorfer, R. Huber, *Nature Photon.* **2010**, *5*, 31.
[11] R. Carley, K. Döbrich, B. Frietsch, C. Gahl, M. Teichmann, O. Schwarzkopf, P. Wernet, M. Weinelt, *Phys. Rev. Lett.* **2012**, *109*, 057401.
[12] R. V. Mikhaylovskiy, E. Hendry, A. Secchi, J. H. Mentink, M. Eckstein, A. Wu, R. V. Pisarev, V. V. Kruglyak, M. I. Katsnelson, T. Rasing, A. V. Kimel, *Nat. Commun.* **2015**, *6*, 8190.
[13] U. Balucani, V. Tognetti, *Phys. Rev. B* **1973**, *8*, 4247.
[14] U. Balucani, V. Tognetti, *Riv. Nuovo Cimento* **1976**, *6*, 39.
[15] D. Fausti, O. V. Misochko, P. H. M. van Loosdrecht, *Phys. Rev. B* **2009**, *80*, 161207.
[16] R. B. Versteeg, J. Zhu, P. Padmanabhan, C. Boguschewski, R. German, M. Goedecke, P. Becker, P. H. M. van Loosdrecht, *Struct. Dyn.* **2018**, *5*, 044301.
[17] S. Mukamel, *Principles of Nonlinear Spectroscopy*, Oxford University Press, Oxford, UK **1995**.
[18] J. S. Baskin, A. H. Zewail, *J. Chem. Educ.* **2001**, *78*, 737.
[19] M. Yoshizawa, M. Kubo, M. Kurosawa, *J. Lumin.* **2000**, *87*, 739.
[20] D. R. Dietze, R. A. Mathies, *ChemPhysChem* **2016**, *17*, 1224.
[21] P. Kukura, D. W. McCamant, R. A. Mathies, *Annu. Rev. Phys. Chem.* **2007**, *58*, 461.
[22] S. Laimgruber, H. Schachenmayr, B. Schmidt, W. Zinth, P. Gilch, *Appl. Phys. B* **2006**, *85*, 557.
[23] C. Fang, R. R. Frontiera, R. Tran, R. A. Mathies, *Nature* **2009**, *462*, 200.
[24] J. Zhou, W. Yu, A. E. Bragg, *J. Phys. Chem. Lett.* **2015**, *6*, 3496.
[25] M. S. Barclay, T. J. Quincy, D. B. Williams-Young, M. Caricato, C. G. Elles, *J. Phys. Chem. AJ. Phys. Chem. A* **2017**, *121*, 7937.
[26] K. Roy, S. Kayal, V. R. Kumar, A. Beeby, F. Ariese, S. Umapathy, *J. Phys. Chem. A* **2017**, *121*, 6538.
[27] M. Quick, A. L. Dobryakov, S. A. Kovalenko, N. P. Ernsting, *J. Phys. Chem. Lett.* **2015**, *6*, 1216.
[28] G. Batignani, E. Pontecorvo, C. Ferrante, M. Aschi, C. G. Elles, T. Scopigno, *J. Phys. Chem. Lett.* **2016**, *7*, 2981.
[29] C. R. Hall, J. Conyard, I. A. Heisler, G. Jones, J. Frost, W. R. Browne, B. L. Feringa, S. R. Meech, *J. Am. Chem. Soc.* **2017**, *139*, 7408.
[30] M. S. Barclay, T. J. Quincy, D. B. Williams-Young, M. Caricato, and C. G. Elles, *J. Phys. Chem. A* **2017**, *121*, 7937.
[31] T. J. Quincy, M. S. Barclay, M. Caricato, and C. G. Elles, *J. Phys. Chem. A* **2018**, *122*, 8308.
[32] Y. Hontani, M. Kloz, T. Polívka, M. K. Shukla, R. Sobotka, J. T. M. Kennis, *J. Phys. Chem. Lett.* **2018**, *9*, 1788.
[33] Z. Piontkowski, D. W. McCamant, *J. Am. Chem. Soc.* **2018**, *140*, 11046.
[34] T. Takaya, M. Anan, K. Iwata, *Phys. Chem. Chem. Phys.* **2018**, *20*, 3320.
[35] M. A. Taylor, L. Zhu, N. D. Rozanov, K. T. Stout, C. Chen, C. Fang, *Phys. Chem. Chem. Phys.* **2019**, *21*, 9728.
[36] D. C. Hannah, K. E. Brown, R. M. Young, M. R. Wasielewski, G. C. Schatz, D. T. Co, R. D. Schaller, *Phys. Rev. Lett.* **2013**, *111*, 107401.
[37] F. Provencher, N. Bérubé, A. W. Parker, G. M. Greetham, M. Towrie, C. Hellmann, M. Côté, N. Stingelin, C. Silva, S. C. Hayes, *Nat. Commun.* **2014**, *5*, 4288.

[38] T. Ghosh, S. Aharon, L. Etgar, S. Ruhman, *J. Am. Chem. Soc.* **2017**, *139*, 18262.
[39] G. Batignani, G. Fumero, A. R. S. Kandada, G. Cerullo, M. Gandini, C. Ferrante, A. Petrozza, T. Scopigno, *Nat. Commun.* **2018**, *9*, 1971.
[40] M. Park, A. J. Neukirch, S. E. Reyes-Lillo, M. Lai, S. R. Ellis, D. Dietze, J. B. Neaton, P. Yang, S. Tretiak, R. A. Mathies, *Nat. Commun.* **2018**, *9*, 2525.
[41] P. Kukura, *Science* **2005**, *310*, 1006.
[42] S. Mukamel, J. D. Biggs, *J. Chem. Phys.* **2011**, *134*, 161101.
[43] G. Fumero, G. Batignani, K. E. Dorfman, S. Mukamel, T. Scopigno, *ChemPhysChem* **2015**, *16*, 3438.
[44] G. Batignani, D. Bossini, N. D. Palo, C. Ferrante, E. Pontecorvo, G. Cerullo, A. Kimel, T. Scopigno, *Nature Photon.* **2015**, *9*, 506.
[45] M. Cinchetti, *Nature Photon.* **2015**, *9*, 489.
[46] S. A. Kovalenko, A. L. Dobryakov, J. Ruthmann, N. P. Ernsting, *Phys. Rev. A* **1999**, *59*, 2369.
[47] M. Liebel, C. Schnedermann, T. Wende, P. Kukura, *J. Phys. Chem. A* **2015**, *119*, 9506.
[48] A. J. Musser, M. Liebel, C. Schnedermann, T. Wende, T. B. Kehoe, A. Rao, P. Kukura, *Nat. Phys.* **2015**, *11*, 352.
[49] L. Monacelli, G. Batignani, G. Fumero, C. Ferrante, S. Mukamel, T. Scopigno, *J. Phys. Chem. Lett.* **2017**, *8*, 966.
[50] G. Batignani, G. Fumero, E. Pontecorvo, C. Ferrante, S. Mukamel, T. Scopigno, *ACS Photonics* **2019**, *6*, 492.
[51] U. Harbola, S. Umapathy, S. Mukamel, *Phys. Rev. A* **2013**, *88*, 011801(R).
[52] G. Batignani, E. Pontecorvo, G. Giovannetti, C. Ferrante, G. Fumero, T. Scopigno, *Sci. Rep.* **2016**, *6*.
[53] G. P. Agrawal, P. L. Baldeck, R. R. Alfano, *Phys. Rev. A* **1989**, *40*, 5063.
[54] G. Agrawal, *Nonlinear Fiber Optics*, Academic Press, London, UK **2013**.
[55] J. Nouet, A. Zarembowitch, R. V. Pisarev, J. Ferre, M. Lecomte, *Appl. Phys. Lett.* **1972**, *21*, 161.
[56] M. G. Cottam, D. J. Lockwood, *Light Scattering in Magnetic Solids*, Wiley, New York **1986**.
[57] S. R. Chinn, H. J. Zeiger, J. R. O'Connor, *Phys. Rev. B* **1971**, *3*, 1709.
[58] D. Bossini, S. D. Conte, Y. Hashimoto, A. Secchi, R. V. Pisarev, T. Rasing, G. Cerullo, A. V. Kimel, *Nat. Commun.* **2016**, *7*, 10645.
[59] S. Yoon, D. W. McCamant, P. Kukura, R. A. Mathies, D. Zhang, S. Y. Lee, *J. Chem. Phys* **2005**, *122*, 024505.
[60] C. Ferrante, G. Batignani, G. Fumero, E. Pontecorvo, A. Virga, L. C. Montemiglio, G. Cerullo, M. H. Vos, T. Scopigno, *J. Raman Spectrosc.* **2018**, *49*, 913.
[61] B. Zhao, K. Niu, X. Li, S. Y. Lee, *Sci. China Chem.* **2011**, *54*, 1989.
[62] G. Batignani, G. Fumero, S. Mukamel, T. Scopigno, *Phys. Chem. Chem. Phys.* **2015**, *17*, 10454.
[63] A. Virga, C. Ferrante, G. Batignani, D. D. Fazio, A. D. G. Nunn, A. C. Ferrari, G. Cerullo, T. Scopigno, *Nat. Commun.* **2019**, *10*, 3658.
[64] R. W. Boyd, *Nonlinear Optics*, 3rd ed., Academic Press, Amsterdam, The Netherlands **2008**.
[65] S. Lim, B. Chon, H. Rhee, M. Cho, *J. Raman Spectrosc.* **2018**, *49*, 607.
[66] P. L. Baldeck, R. R. Alfano, G. P. Agrawal, *Appl. Phys. Lett.* **1988**, *52*, 1939.
[67] R. J. Elliott, M. F. Thorpe, *J. Phys. C* **1969**, *2*, 1630.
[68] S. D. Conte, C. Giannetti, G. Coslovich, F. Cilento, D. Bossini, T. Abebaw, F. Banfi, G. Ferrini, H. Eisaki, M. Greven, A. Damascelli, D. van der Marel, F. Parmigiani, *Science* **2012**, *335*, 1600.